

Unifying MeV-Blazars with GeV-Blazars

M. Blazejowski *et al.*

Presented at the Stellar Coronae in the Chandra and the XMM Newton Era,
6/25/2001—6/29/2001, Noordwijk, The Netherlands

Stanford Linear Accelerator Center, Stanford University, Stanford, CA 94309

Work supported by Department of Energy contract DE-AC03-76SF00515.

UNIFYING MEV-BLAZARS WITH GEV-BLAZARS

M. Błażejowski¹, M. Sikora^{1,2}, R. Moderski¹, and G. Madejski²

¹Nicolaus Copernicus Astronomical Center, Warsaw, POLAND

²Stanford Linear Accelerator Center Menlo Park, CA 94025, USA

ABSTRACT

We demonstrate that the spectral differences between Flat Spectrum Radio Quasars (FSRQ) with steep gamma-ray spectra (MeV-blazars) and FSRQ with flat gamma-ray spectra (GeV-blazars) can be explained by assuming that in the MeV-blazars, the production of gamma-rays is dominated by Comptonization of infrared radiation of hot dust, whereas in the GeV-blazars — by Comptonization of broad emission lines. Additional ingredient, required to reach satisfactory unification, is an assumption that the radiating electrons are accelerated via a two step process, in the lower energy range – following instabilities driven by shock-reflected ions, and in the higher energy range – via resonant scatterings off Alfvén waves. Our model predicts that on average, the MeV-blazars should vary on longer time scales than GeV-blazars.

Key words: Missions: XMM-Newton – blazars, jets

1. ASSUMPTIONS

- Relativistic electrons in a subparsec jet are produced in shocks formed by colliding inhomogeneities. The inhomogeneities are assumed to be intrinsically identical and to move down the jet with bulk Lorentz factors $\Gamma_2 > \Gamma_1 \gg 1$;
- Time scale of the collision, as measured in the comoving frame of the shocked plasma, is

$$t'_{coll} \simeq t_{fi} \mathcal{D}, \quad (1)$$

where t_{fi} is the observed time scale of the flare, and

$$\mathcal{D} \equiv \frac{1}{\Gamma(1 - \beta \cos \theta_{obs})} \quad (2)$$

is the Doppler factor of the shocked plasma, and

$$\Gamma \simeq \sqrt{\Gamma_1 \Gamma_2}; \quad (3)$$

- Inertia of inhomogeneities is dominated by protons (i.e. $n_e/n_p \ll m_p/m_e$);
- Efficiency of energy dissipation is defined as

$$\eta_{diss} \simeq \frac{((\Gamma_2/\Gamma_1)^{1/2} - 1)^2}{(\Gamma_2/\Gamma_1) + 1}, \quad (4)$$

- Injection of relativistic electrons is approximated by a two-power-law function, with the break at γ_b , at which magnetic rigidity of electrons is equal to rigidity of thermal protons, i.e., when their momenta are equal

$$m_e \sqrt{\gamma_b^2 - 1} \simeq m_p \sqrt{\gamma_{p,th}^2 - 1}, \quad (5)$$

where

$$\gamma_{p,th} - 1 = \eta_{p,th} \kappa \quad (6)$$

is the average thermal proton energy in the shocked plasma, $\eta_{p,th}$ is the fraction of the dissipated energy tapped to heat the protons and

$$\kappa \simeq \frac{((\Gamma_2/\Gamma_1)^{1/2} - 1)^2}{2(\Gamma_2/\Gamma_1)^{1/2}}. \quad (7)$$

is the amount of energy dissipated per proton in units of $m_p c^2$.

- Since the time scales of the flares in FSRQ are rarely shorter than 1 day, the distances of their production,

$$r_{fl} \sim (r_{fl}/\Delta r_{coll}) c t_{fi} \mathcal{D} \Gamma \quad (8)$$

are expected to be larger than 0.1 parsec (where Δr_{coll} is a distance range over which the flare is produced). At such distances, the largest contribution to the energy density of an external radiation field u'_{ext} is provided by the diffuse component of the broad emission lines and infrared radiation of hot dust.

2. SPECTRA

The basic feature of the high energy spectra in FSRQ — a break between the γ -ray and the X-ray spectral portions — has a natural explanation in terms of the External Radiation Comptonization (ERC) model (Sikora et al. 1994). In this model, X-ray spectra are produced by electrons with radiative cooling time scale, t'_{cool} , longer than the collision time scale, t'_{coll} (*slow cooling regime*), whereas γ -rays are produced by electrons with $t'_{cool} < t'_{coll}$ (*fast cooling regime*). Noting that cooling rate of electrons, dominated by Comptonization of external radiation, is

$$\dot{\gamma} \simeq \frac{c\sigma_T}{m_e c^2} u'_{ext} \gamma^2 \quad (9)$$

we obtain that cooling time scale is

$$t'_{cool} \simeq \frac{\gamma}{\dot{\gamma}} \simeq \frac{m_e c^2}{c\sigma_T} \frac{1}{\gamma u'_{ext}} \quad (10)$$

where u'_{ext} is the energy density of an external radiation field. Then, from $t'_{cool} = t'_{coll}$, where t'_{coll} is given by Eq. (1), the break in the electron distribution is

$$\gamma_c \simeq \frac{m_e c^2}{c \sigma_T u'_{ext} t_{fl} \Gamma^2} \quad (11)$$

For $\gamma < \gamma_c$, the slope of the electron distribution is the same as the slope of the injection function, while for $\gamma > \gamma_c$, the slope of the electron energy distribution is steeper by $\Delta s = 1$ ($s : N_\gamma \propto \gamma^{-s}$).

For $u'_{ext} \simeq u_{diff} \Gamma^2$, we predict that the break in an electron energy distribution at γ_c should be imprinted in the electromagnetic spectrum at frequency

$$\nu_c \sim \Gamma^2 \gamma_c^2 \nu_{diff} \simeq \left(\frac{m_e c^2}{\sigma_T} \right)^2 \frac{\nu_{diff}}{u_{diff}^2 \Delta r_{coll}^2}, \quad (12)$$

where ν_{diff} is the characteristic frequency of the diffuse external radiation field.

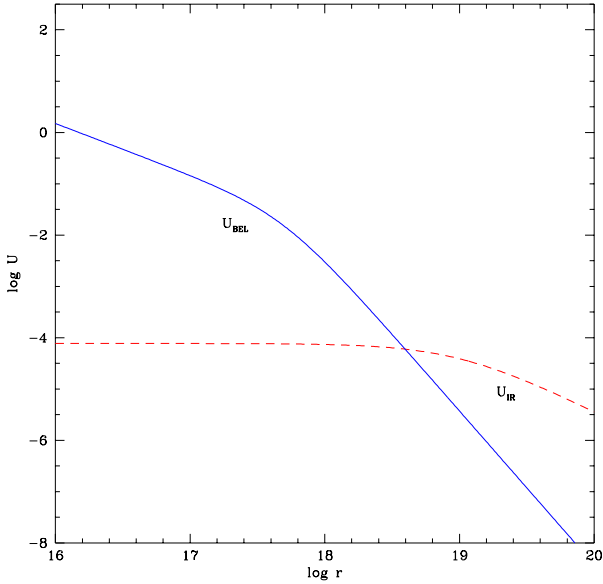


Figure 1. The dependence of energy density of u_{BEL} (solid line) and u_{IR} (dashed line) on distance from the central source is shown.

The predicted location of the break does not depend on Γ , and, for typical energy densities of BELR and of the hot dust radiation, is comparable to the range $10^{20} - 10^{22}$ Hz determined from observations (see Fig. 2). The presented results are obtained using the following approximations for energy densities of the diffused external radiation components:

$$u_{BEL,diff}(r) \simeq \frac{\xi_{BEL}(r_{BEL}) L_{UV}}{4\pi r^2 ((r/r_{BEL}) + (r_{BEL}/r)) c} \quad (13)$$

where

$$r_{BEL} \sim 3 \times 10^{17} \sqrt{L_{UV,46} \text{ cm}} \quad (14)$$

and

$$u_{IR,diff}(r) \simeq \frac{\xi_{IR}(r_{d,min}) L_{UV}}{4\pi (r_{d,min}^2 + r^2 (r_{d,min}/r)^{-0.68}) c} \quad (15)$$

where

$$r_{d,min} \simeq \left(\frac{L_{UV}}{4\pi \sigma_{SB} T_{d,max}^4} \right)^{1/2} \quad (16)$$

is the minimum distance of dust to the central source and $T_{d,max}$ is the maximum temperature of dust.

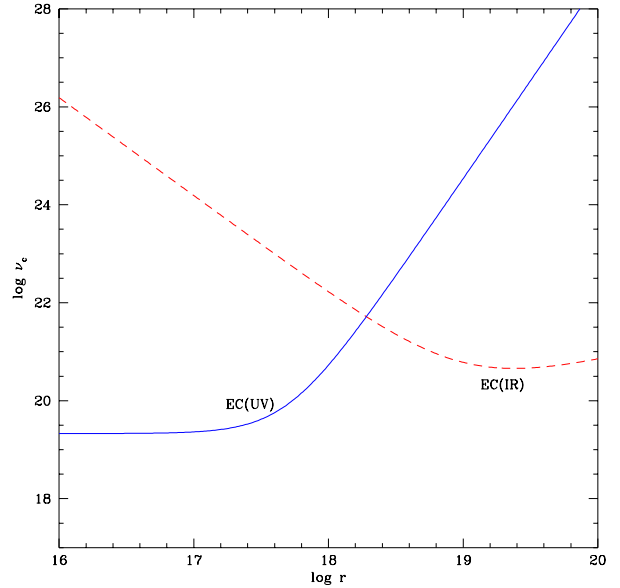


Figure 2. The dependence of ν_c on the distance. Solid line- $\nu_{EC(UV),c}$, dashed line- $\nu_{EC(IR),c}$.

Due to the cooling effect the spectra should have a break by $\Delta\alpha = 0.5$, and this is consistent with the spectral breaks observed in γ -ray quasars during flares. In these quasars, the spectral index in the EGRET range is $\alpha_\gamma \leq 1$ (Pohl et al. 1997). There are, however, several quasars, called MeV-blazars, which have the spectral break $\Delta\alpha$ much larger than 0.5. Their γ -ray spectra are very soft, with $\alpha_\gamma \geq 1.5$, and the X-ray spectra are very hard, with $\alpha_X \leq 0.5$ (Tavecchio et al. 2000). In order to explain such spectra, it is necessary to postulate the break in the electron injection function. Origin of the break can be related to the two-step acceleration process of electrons and its location is likely to be at γ_b (see Eq.(5)). For $2.5 < \Gamma_2/\Gamma_1 < 10$ and $\eta_{p,th} = 0.5$, the break in the electron injection function is $600 < \gamma_b < 1700$.

External photons scattered by electrons with Lorentz factors γ_b are boosted up to energies

$$\nu_b \sim \gamma_b^2 \Gamma^2 \nu_{ext} \quad (17)$$

Hence, the break in the electron injection function is imprinted in the electromagnetic spectrum at around 1 GeV

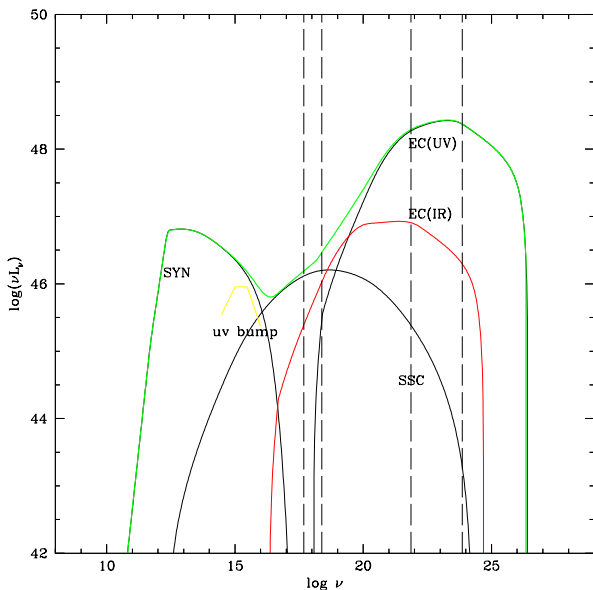


Figure 3. The broadband spectrum of a “typical” GeV-blazar (for the justification of the parameters used in the model, see Sikora et al. 2002 in preparation). The two areas confined by vertical dashed lines represent 2 – 10 keV and 30 MeV - 3 GeV bands respectively.

if $\nu_{ext} = \nu_{BEL}$, and at ten times lower energies, if $\nu_{ext} = \nu_{IR}$. In the former case $\nu_b \gg \nu_c$ and the γ -ray spectra in the EGRET range have slopes $\alpha_\gamma \leq 1$ (see Fig.(3)), while in the latter case $\nu_b \sim \nu_c \leq 30$ MeV, and the γ -ray spectra in the EGRET range are very soft (see Fig.(4)).

The above scheme can also explain two other differences between MeV-blazars and GeV-blazars. One is that in MeV-blazars, the contribution to the spectra from thermal UV-bump is often more apparent than in GeV-blazars (see, e.g., Tavecchio et al. 2000), and the other is that the X-ray spectra are harder in MeV-blazars than in GeV blazars. The former results in our model from the fact that due to the decrease of magnetic field with distance, the break in the electron synchrotron spectrum at $\nu_{syn,b}$ is shifted to lower frequencies at larger distances, and the dilution of thermal UV radiation by synchrotron component is reduced. The latter is a result of the fact that the SSC spectrum is produced at larger distances and thus it is shifted to lower frequencies and has lower intensity; furthermore, at those distances, the dust covering factor is larger than the BELR covering factor.

Additional prediction of our scheme is that time scales of flares produced in MeV blazars should on average be longer than the time scales of flares produced in GeV blazars. With the planned sensitive gamma-ray observatories such as GLAST, this prediction can be verified in future statistically, but also via studies of individual objects such as PKS 0208-512, which sometimes show very

hard γ -ray spectra and on other occasions — very soft γ -ray spectra (Blom et al. 1996, Stacy et al. 1996).

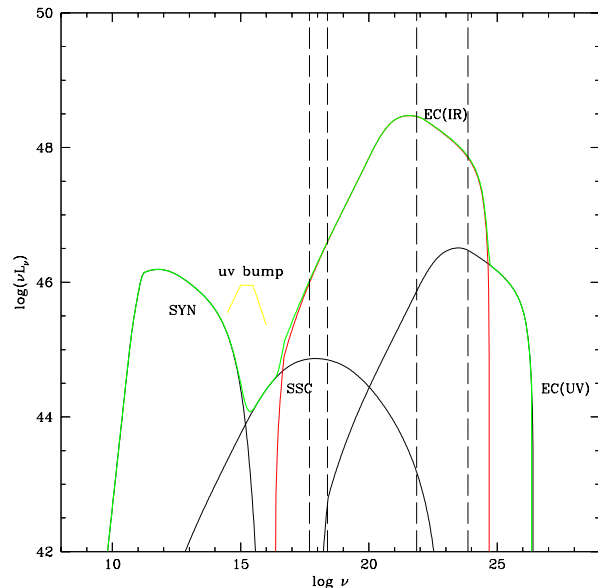


Figure 4. The broadband spectrum of a “typical” MeV-blazar.

ACKNOWLEDGEMENTS

This work was partially supported by the Polish Committee of Scientific Research grant no. 5 P03D 002 21, and by NASA Chandra grant GO0 - 1038A to Stanford University.

REFERENCES

- Blom J.J. et al. 1996 A&A Suppl.Ser. 120, 507.
- Pohl M., et al. 1997 A&A, 326, 51.
- Sikora M., Begelman M.C., Rees M.J., 1994, ApJ, 421, 153.
- Stacy J.G. et al. 1996 A&A Suppl.Ser.120, 549.
- Tavecchio F. et al. 2000 ApJ, 544, L23.